Journal of Coordination Chemistry

ISSN: (Print) (Online) Journal homepage: https://www.tandfonline.com/loi/gcoo20

Solvatochromic behavior of a pyrene-pyrimidine-based Schiff base and detection of heavy metal ions in aqueous media

Swadesh Ghosh, Dipti Singharoy, Saugata Konar, Jnan Prakash Naskar & Subhash Chandra Bhattacharya

To cite this article: Swadesh Ghosh, Dipti Singharoy, Saugata Konar, Jnan Prakash Naskar & Subhash Chandra Bhattacharya (2021) Solvatochromic behavior of a pyrene-pyrimidine-based Schiff base and detection of heavy metal ions in aqueous media, Journal of Coordination Chemistry, 74:8, 1272-1283, DOI: 10.1080/00958972.2021.1897980

To link to this article: https://doi.org/10.1080/00958972.2021.1897980

JOURNAL OF COORDINATION CHEMISTRY
2021, VOL. 74, NO. 8, 1272–1283
https://doi.org/10.1080/00958972.2021.1897980

Solvatochromic behavior of a pyrene-pyrimidine-based Schiff base and detection of heavy metal ions in aqueous media

Swadesh Ghosh[a], Dipti Singharoy[a], Saugata Konar[b], Jnan Prakash Naskar[a] and Subhash Chandra Bhattacharya[a]

[a]Department of Chemistry, Jadavpur University, Kolkata, India; [b]Department of Chemistry, The Bhawanipur Education Society College, Kolkata, India

ABSTRACT

The synthesis and solvatochromic behavior of pyrimidine based Schiff-base (PYPH) were studied to develop a fluorescent chemo sensor for the detection of Hg^{2+} in aqueous solution. The characterization of PYPH was investigated on the basis of UV–vis, FTIR, ^{1}H-NMR and mass spectral data. PYPH displays selective fluorescent turn-off response to Hg^{2+} in aqueous solution. The sensitivity and selectivity of PYPH toward Hg^{2+} among different metal ions was examined by absorption, fluorescence, ^{1}H-NMR and mass spectral studies. Binding stoichiometry (2:1) has been confirmed by a Job's plot, HRMS spectral studies and ^{1}H-NMR analysis. A low detection limit was 4.2×10^{-6} M for Hg^{2+}. Ground state geometry of PYPH has been optimized using density functional theory (DFT). These results demonstrate that PYPH has promise to detect Hg^{2+} ion in environmental analysis systems.

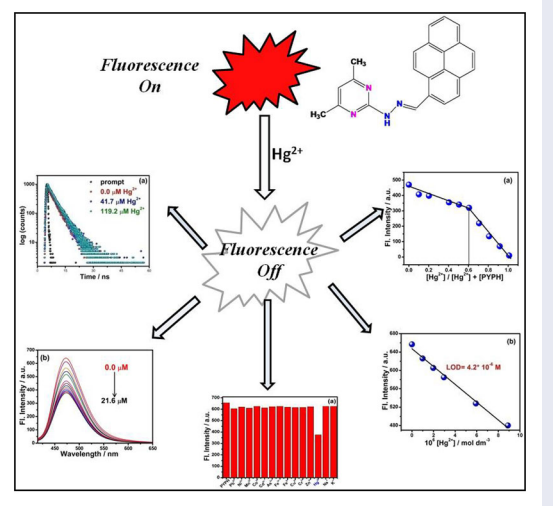

ARTICLE HISTORY
Received 13 July 2020
Accepted 26 January 2021

KEYWORDS
Synthesis; solvent study; mercury detection; selectivity

CONTACT Subhash Chandra Bhattacharya sbjuchem@yahoo.com, scbhattacharyya@chemistry.jdvu.ac.in; Jnan Prakash Naskar jpnaskar@rediffmail.com Department of Chemistry, Jadavpur University, Kolkata, 700032 India

Supplemental data for this article is available online at https://doi.org/10.1080/00958972.2021.1897980.

1. Introduction

Sensing and reporting of chemical species is of major importance [1]. Metals are present in living or non-living species. Some metals, e.g., iron, copper, zinc are essential for biological processes and enzymatic reactions that occur in the human body; conversely some metals are unsafe for living organisms. Among them mercury is a heavy metal occurring in different forms, all of which can produce deadly toxic effects in the human body. Zero oxidation state of Hg exists as vapor or as liquid metal, +1 oxidation state of Hg exists as inorganic salts and +2 oxidation state of Hg may form either inorganic salts or organomercury compounds; the three oxidation states differ in toxic effects [2]. Even at a low concentration, mercury is one of the most dangerous metal ions for the ecosystem [3]. It can accumulate in a human body through the food chain leading to many diseases, nervous system defects, erythrism, arrhythmia, cardiomyopathy, and kidney damage [4–8]. Mercury shows high permeability to skin and seriously damages respiratory, gastrointestinal and excretory systems, prenatal brain damage, serious cognitive, motion disorders, deafness, minamata and alzheimer [9, 10]. Additionally, it shows a high affinity for thiol groups in proteins and leads to the malfunction of cells and consequently leads to many diseases [11]. Due to its affinity for sulfhydryl and thiol groups, it can change the macromolecular structure and also damage DNA [12]. Mercury has been shown to induce oxidative stress and mitochondrial dysfunction [13] resulting in alterations in calcium homeostasis and increased lipid peroxidation [14]. Mercury may also increase radical oxygen species levels because of its ability to act as a catalyst. Therefore, the need for highly sensitive and selective determination of mercury ions is of importance.

Pyrimidine containing Schiff bases are promising with broad spectrum of biological activity and for the detection of toxic heavy metal ions [15]. To develop the Schiff base as a sensor, pyrene derivatives are widely used due to their excellent photoluminescence and chemical stabilities. Among heterocycles, pyrimidines represent a particularly important class of compounds due to their diverse applications for pharmaceutical properties. Schiff bases have biological activity, such as antitumor [16, 17], anticancer [18], antifungal, and antimicrobial activities [19–21]. Biological activity is related to hydrogen bonding through the imino group of Schiff bases with the active centers of the cell constituents [22]. Based on these factors we focus on Schiff bases, which are prepared using simple steps and can be applied to many cation and anion sensors. Pyrimidine is the structural unit of DNA and RNA playing a vital role with the most abundant pyrimidines uracil, cytosine and thymine. Pyrene has also a remarkable range of biological activity as anti-bacterial agents, [23] anti-tumor [24] and anti-fungal [25] compounds.

In this study, due to biological significance of pyrimidines we have synthesized a pyrimidine based Schiff base ligand 2-(4,6-dimethylpyrimidin-2-yl)-1-((pyren-8-yl)methylene)hydrazine (PYPH) as a new chemosensor for detection of Hg^{2+}. There are many mercury ion sensor Schiff bases but the biologically active pyrimidine moiety in the Schiff base was absent. The influences of solvent on absorbance and fluorescence spectra of PYPH are reported and it shows high selectivity and sensitivity to Hg^{2+} over other metal ions. Selective and sensitive detection of PYPH towards Hg^{2+} has been confirmed by absorbance, fluorescence, ^{1}H-NMR titration and HRMS spectroscopic

studies. The present system is simple, cost effective and sensitive towards Hg^{2+} ion which may be employed in eco-friendly aqueous medium.

2. Experimental

2.1. Materials

The spectral grade solvents ethanol (EtOH), methanol (MeOH), conc. HCl, 1-pyrene carboxaldehyde, phosphorous oxy chloride ($POCl_3$), acetyl acetone, hydrazine hydrate, potassium bromide (KBr) and urea were purchased from E. Merck, India. Solvents were purified and dried according to standard methods [26] and used only after checking their purity fluorimetrically in the wavelength range of interest. DMSO-d_6 as received from Sigma-Aldrich, USA was used for ^{1}H-NMR experiments. Perchlorate salts of Fe^{3+}, Co^{2+}, Cd^{2+}, Hg^{2+}, Ni^{2+} and Zn^{2+} were purchased from Sigma-Aldrich and other metal salts like $Al(NO_3)_3$, $CrCl_3$, $MnCl_2$ and $Cu(ClO_4)_2$ were procured from commercial sources (SRL); all were used as received. Millipore water was used throughout the experiments.

2.2. Synthesis

2.2.1. Synthesis of 2-(4,6-dimethylpyrimidin-2-yl)-1-((pyren-8-yl)methylene)hydrazine (PYPH)

PYPH was synthesized by refluxing an ethanolic solution (20 ml) of 4,6-dimethyl 2-hydrazino pyrimidine (10 mmol, 1.39 g) [27–29] with 1-pyrenecarboxaldehyde (10 mmol, 2.30 g) also in ethanol (20 ml). Reflux was continued for 2 h at water bath temperature during which a solid compound separated. It was filtered, washed with ethanol and dried over fused $CaCl_2$. The crude product was recrystallized from ethanol–water mixture. It is soluble in DMSO, DMF, THF and MeCN but insoluble in MeOH, DCM, $CHCl_3$, n-hexane and n-pentane. (Yield: 79.30%); Anal. Calc. for $C_{23}H_{18}N_4$: C, 78.86; H, 5.14; N, 16.00. Found: C, 78.79; H, 5.10; N, 16.05%. ^{1}H-NMR (in d_6-DMSO, 300 MHz) δ 11.33 (1H, s), 9.17 (1H, s), 8.73 (1H, J = 9 Hz, 1H), 8.55 (1H, J = 8 Hz, 1H), 8.33-8.06 (m, 7H), 6.66 (1H, S), 2.354 (s, 6H) (Figure S1, supplementary material). ESI-MS: m/z calculated for $C_{23}H_{18}N_4$ $[PYPH + H]^+$ 351.15, found 351.26 (Figure S2, supplementary material); IR (KBr, cm-1) υ: 3417 (N-H), 1667 (C = N) (Figure S3, supplementary material).

2.2.2. Synthesis and formulation

PYPH is a 1:1 molar Schiff base condensate of 4,6-dimethyl 2-hydrazino pyrimidine and 1-pyrenecarboxaldehyde in EtOH. PYPH was spectroscopically characterized by FT-IR, ESI-MS and ^{1}H-NMR. In Scheme 1, the synthetic scheme of PYPH is outlined.

2.3. Methods

^{1}H-NMR spectra were obtained with a Bruker Avance DPX 300 spectrometer using DMSO-d_6 solution. Infrared spectra ($4000 - 400\,cm^{-1}$) were taken as KBr pellets using a Perkin Elmer Spectrum BX-II IR spectrometer. Mass spectroscopic analysis of PYPH was obtained from a QTOF Micro YA263 ESI-TOF mass spectrometer using methanol

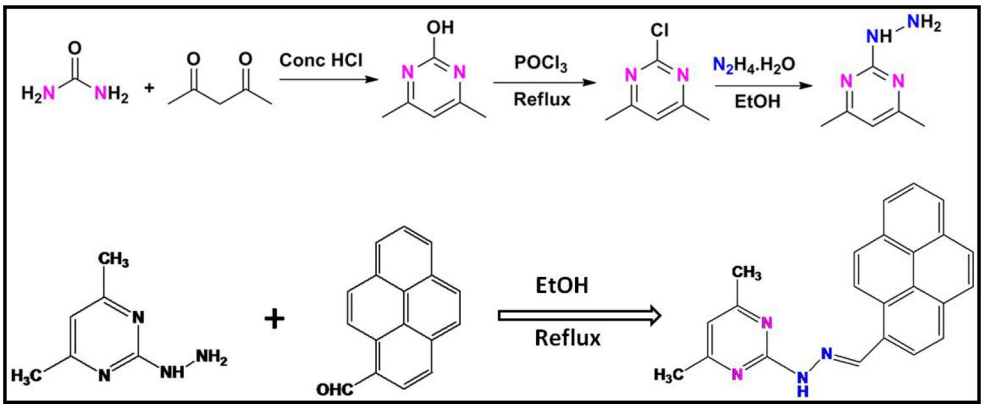

Scheme 1. Synthesis outline of PYPH.

as solvent. Elemental analyses (carbon, hydrogen and nitrogen) were obtained from a Perkin Elmer CHN analyzer 2400. Absorption and fluorescence spectra were recorded using a Shimadzu (model UV1700) UV–vis spectrophotometer and Shimadzu spectrofluroimeter (model RF 5301), respectively. Fluorescence decay curves were obtained from time resolved intensity decay by time-correlated single photon counting (TCSPC) using a nanosecond diode LED at 370 nm (IBH, nano LED) as a light source. The data stored in a multichannel analyzer were routinely transferred to IBH DAS-6 decay analysis software. For lifetime measurements, the fluorescence decay curves were analyzed by an exponential iterative fitting program provided by IBH using Eq. (1),

$$F(t) = \sum_i \alpha_i \exp\left(^{-t}/_{\tau_i}\right) \quad (1)$$

where α_i is the pre exponential factor representing the fractional contribution to the time resolved decay of the component with lifetime. Ground state geometries of PYPH were optimized employing density functional theory [30, 31] using the B3LYP [32, 33] functional with the standard basis set, 6-311 G (d, p), for all atoms in the Gaussian 09 program [34].

3. Results and discussion

3.1. Solvent modulated properties of PYPH

Absorption and emission spectra of PYPH has been studied in solvents of different polarity. Absorption spectra of PYPH (Figure 1(a)) have a broad band with a maximum between 384 and 405 nm (Table 1) in the solvents of different polarity (H_2O to CyHex, respectively). This band can be ascribed to π-π^* transition to singly excited state (S_1) of molecule. The absorption is intense and peak position is sensitive to the polarity of the medium. The typical solvent shift on changing the polarity of solvents suggests that the ground state of the molecule is polar.

Emission spectra of PYPH, recorded in solvents of different polarity, are represented in Figure 1b. On excitation of PYPH at the absorption maxima in the corresponding solvents, an emission band appears at 470-441 nm. The intensity of the band is low in

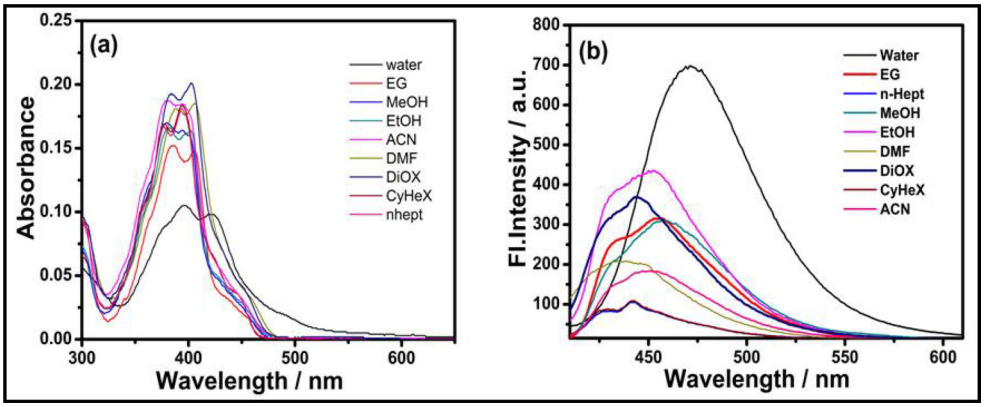

Figure 1. (a) Absorption and (b) emission spectra of PYPH in different homogeneous solvents.

Table 1. Absorbance maximum (λ_{abs}), fluorescence maximum (λ_{fl}), stokes shift ($\Delta\nu$) and E_T (30) values in different homogeneous solvents.[a]

Solvents	λ_{abs} /nm	λ_{fl} /nm	$\Delta\ \nu$ (cm^{-1})	$E_T(30)$ (kcal/mol)
H_2O	398	470	3849	63.1
EG	385	454	3947	56.3
MeOH	384	458	4207	55.4
EtOH	384	456	4111	51.9
ACN	380	453	4240	46.0
DMF	384	443	3468	43.8
DiOX	385	436	3038	36.0
n-hept	393	442	2820	31.1
Cyhex	393	441	2769	30.9

[a]ACN = acetonitrile, DiOX = dioxane, n-hept = n-heptane.

nonpolar solvents (Figure 1(b)) but with increase of polarity fluorescence intensity is increased. A red shifted fluorescence is observed on increasing solvent polarity. The effect of the polarity of the medium on the fluorescence maximum is greater than that on the absorption maximum. This observation suggested that the emitting state of PYPH is more polar than the ground state.

A plot of Stokes shift ($\Delta\nu$ = difference between transition energy of absorption maxima E(A) and fluorescence maxima E(F)) versus the microscopic solvent polarity parameter, $E_T(30)$ [35], is presented in Figure S4 (supplementary material) where Stokes shift increases sharply from cyclohexane (CyHex) to MeOH and then decreases steeply on changing from ethylene glycol (EG) to water. PYPH exhibits an overall increase in Stokes shift from nonpolar to polar solvents (except water and EG) due to increasing polarity of the medium. Changing the medium from nonpolar to polar stabilizes the excited state of PYPH, which causes a red shift and consequently, Stokes shift increases. But in water and EG, the Stokes shift is decreased due to strong intermolecular hydrogen bonding interactions.

In addition steady state anisotropy of PYPH has been investigated in fully saturated condition of different types of solvent (polar protic, H_2O; polar aprotic, ACN and nonpolar, n-hexane (n-hex)). Steady state fluorescence anisotropy helps to understand the

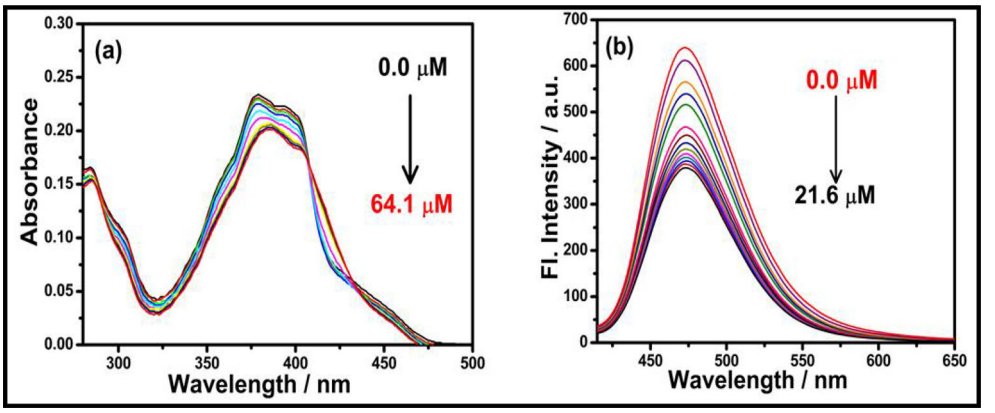

Figure 2. (a) Absorption spectra of PYPH upon addition of Hg^{2+} ions up to 64.1 μM; (b) emission spectra of PYPH upon addition of Hg^{2+} ions up to 21.6 μM.

motional restriction of the molecule due to interaction with different solvents. The anisotropy of PYPH is 0.12 in aqueous media whereas the anisotropy of PYPH is 0.02 and 0.05, respectively, in acetonitrile and n-hex (Figure S5, supplementary material). Hence, anisotropy of PYPH in water is greater than that of polar aprotic ACN and non-polar n-hex solvents, supporting that strong intermolecular hydrogen bonding interaction takes place. Hydrophobic interaction of PYPH in non-polar solvent indicates higher anisotropy of PYPH than polar aprotic solvents. Time-resolved fluorescence measurements were performed for PYPH in three different solvents to characterize the spectral properties and dynamics, considering the polarity in the excited state (Table S1, supplementary material). The excited state decay profiles in different homogeneous environments are shown in Figure S6 (supplementary material) which has been fitted with a single exponential decay with χ^2 value near one (Table S1, supplementary material). Fluorescence lifetime values of PYPH increases with polarity of solvents and lies between 3.8 and 4.7 ns. Lifetime value of PYPH in water is higher than that in other solvents, which supports the higher fluorescence intensity of PYPH in water.

3.2. Absorbance and emission studies

The absorption spectra of PYPH (9.1 μM) were recorded with λ_{abs} at 398 nm in H_2O due to a π-π* transition. Upon stepwise addition of Hg^{2+} (up to 64.1 μM) to solution of PYPH, absorbance of PYPH decreased (Figure 2(a)). No significant spectral change of PYPH was observed due to addition of other metal cations Na^+, K^+, Ca^{2+}, Co^{2+}, Ni^{2+}, Cu^{2+}, Zn^{2+}, Fe^{3+}, Pb^{2+}, Ag^+, Cd^{2+}, Al^{3+}, Zn^{2+}, Cr^{3+} and Fe^{2+}. The absorbance decrease indicates that ground state interaction takes place between PYPH and Hg^{2+}. To understand selectivity of PYPH towards Hg^{2+}, under similar circumstances in the presence of other metal cations, the fluorescence intensity changes were systematically studied in aqueous medium. On excitation at 398 nm, PYPH showed a strong emission band at 470 nm (λ_{em}). Upon addition of Hg^{2+} (up to 21.6 μM) to solution of PYPH (9.1 μM), the fluorescence of PYPH was quenched at 470 nm with a red shift of 10 nm (Figure 2(b)), indicating formation of complex between PYPH and Hg^{2+}. With the presence of other metal ions, such as Co^{2+}, Ni^{2+}, Hg^{2+}, Fe^{3+}, Cu^{2+}, Zn^{2+}, Cd^{2+},

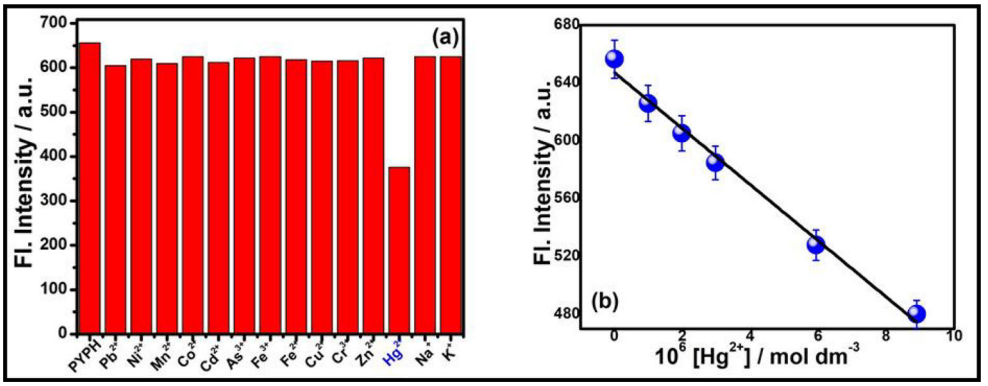

Figure 3. (a) Bar diagram indicates the emission intensity of PYPH (4.97 μM) and concentration of all metal ions (M^{2+} and M^{3+}) are 9.92 μM. (b) Plot of fluorescence intensity of PYPH (9.9 μM) vs. concentration of Hg^{2+} with an error bar (4.6%).

Al^{3+}, Zn^{2+}, Cr^{3+} and Fe^{2+}, no change in fluorescence intensity (shown in bar diagram of Figure 3(a)) has been observed.

The quenching of fluorescence of PYPH with the addition of Hg^{2+} occurs due to non-fluorescent complex formation with metal ions [36–40]. The limit of detection (LOD) of Hg^{2+} by PYPH has been calculated by the 3σ method [41] (LOD = 3σ/m where 'σ' and 'm' are the standard deviation of blank and the slope of the fluorescence intensity vs. concentration of Hg^{2+} plot, respectively, Figure 3(b)) and the value is 4.2×10^{-6} M.

3.3. Binding studies

In order to determine the binding stoichiometry between PYPH and Hg^{2+}, a Job's plot was performed with fluorescence intensity data. From the Job's plot (Figure 4(a)), intensity minima were observed at 0.61 mole fraction, indicating 2:1 stoichiometry complex was formed. This was further confirmed by ESI mass spectra of the complex in methanol. ESI mass spectral peak at m/z = 937.87 for $[C_{46}H_{34}HgN_4+K]^+$ supported the 2:1 stoichiometry of the complex (Figure S7, supplementary material).

Fluorescence spectra were also used for determination of binding constant values between PYPH and Hg^{2+} using the Benesi–Hildebrand (B–H) equation [42] (eq. 2),

$$\frac{1}{I_f - I_{f^0}} = \frac{1}{I_{f/} - I_{f^0}} + \frac{1}{K(I_{f/} - I_{f^0})[Hg^{2+}]} \tag{2}$$

where K is binding constant, I_f^0 is initial fluorescence intensity of free host, I_f is the intermediate fluorescence intensity of PYPH:Hg^{2+} and $I_f{}^{/}$is the maximum fluorescence intensity of the PYPH:Hg^{2+} adduct formed. A plot of $1/(I_f\text{-}I_{f0})$ vs. $1/[Hg^{2+}]$ provides a straight line through the entire range of Hg^{2+} concentration (Figure 4(b)), indicating a 2:1 adduct. From the slope of B-H plot calculated binding constant values for complex formation is 4.1×10^4 M^{-1}. Both results suggested that the receptor PYPH was sensitive towards mercuric ion.

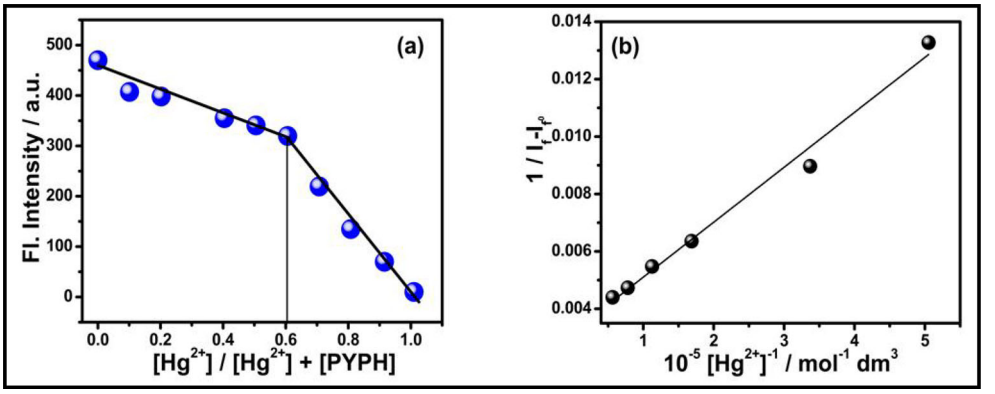

Figure 4. (a) Jobs' plot of PYPH:Hg^{2+} system from fluorescence spectra. (b) B–H plot from the emission spectra of PYPH:Hg^{2+}.

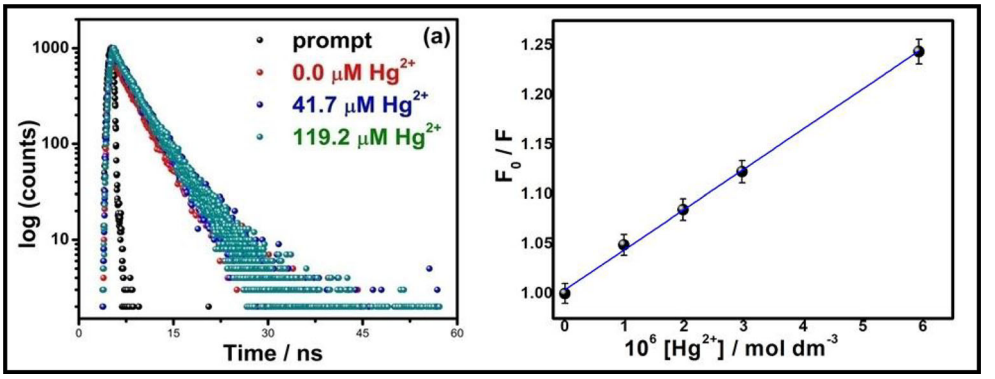

Figure 5. (a) Time resolved fluorescence decay of PYPH upon addition of Hg^{2+} up to 119.2 μM; (b) plot of F_0/F vs. [Hg^{2+}] with an error bar (6.25%).

3.4. Quenching mechanism

We studied the time resolved fluorescence measurement to understand fluorescence quenching process of PYPH. Fluorescence lifetime serves as a sensitive parameter to investigate the environment around a fluorophore, and it is sensitive to excited state interactions. There was no change of fluorescence lifetime of PYPH upon addition of Hg^{2+} ions (Figure 5(a)). Quenching of fluorescence intensity of PYPH with the addition of Hg^{2+} may be due to static quenching. The quenching of fluorescence of PYPH with addition of Hg^{2+} was analyzed by the Stern–Volmer equation (eq. 3) [43],

$$\frac{F_0}{F} = 1 + K_{SV}[Q] \tag{3}$$

where F_0 and F are fluorescence intensities of PYPH in the absence and presence of Hg^{2+} ions, respectively, K_{SV} is the Stern-Volmer constant and [Q] is the Hg^{2+} concentration. A linear curve in the Stern–Volmer plot (Figure 5(b)) was obtained. The K_{SV} value for PYPH is 4.0×10^4 mol dm^{-3}, which also agrees with binding constant value.

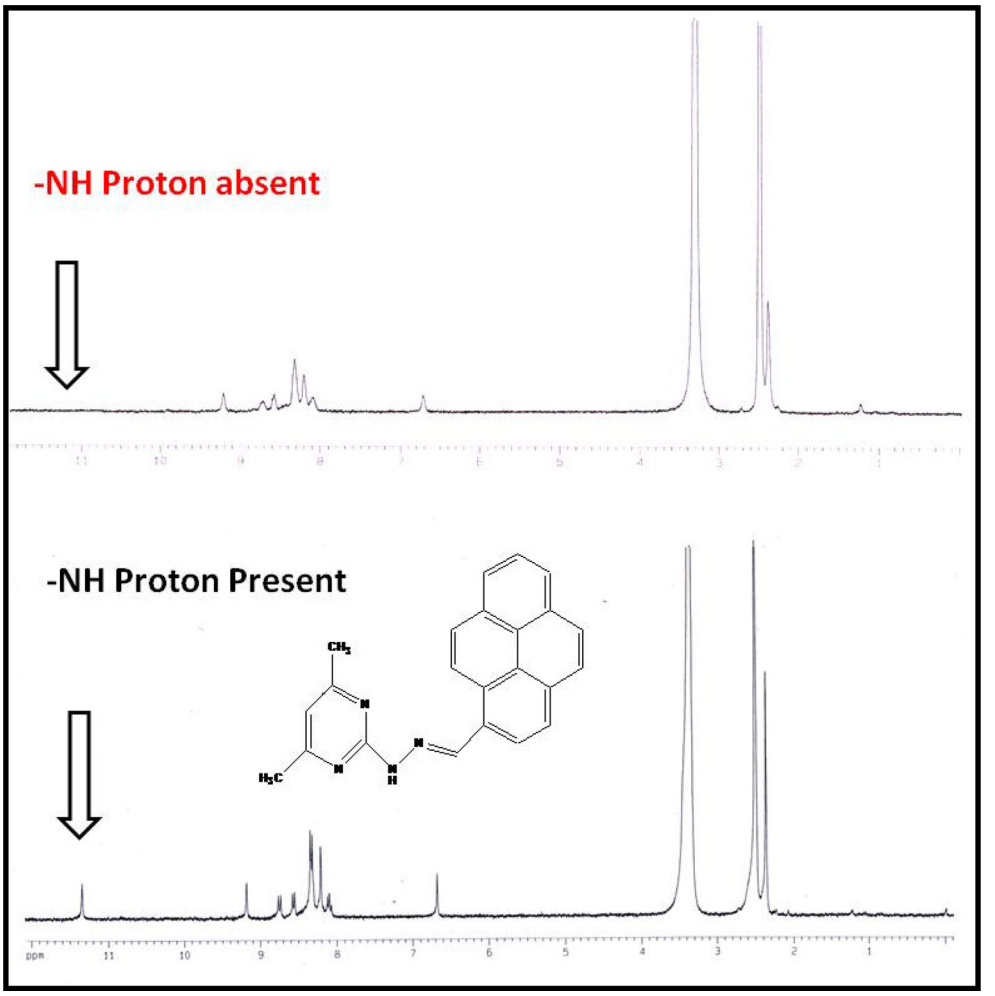

Figure 6. ^{1}H-NMR spectra of PYPH and PYPH with Hg^{2+} ions in DMSO-d_6.

3.5. ^{1}H-NMR titration of complex

To establish possible binding mode of PYPH, ^{1}H-NMR titration experiment was carried out. Proton NMR spectra of PYPH were recorded in the absence and presence of Hg^{2+} in DMSO-d_6 (Figure 6). The -NH proton of PYPH appeared at 11.0 ppm (Figure 6) but with addition of Hg^{2+} to PYPH solution, it disappeared (Figure 6); all the protons of PYPH displayed a slightly upfield shift except the -NH proton. These observations clearly indicate that Hg^{2+} coordinated to the N of –NH group after deprotonation to satisfy the primary and secondary valency. This has been further supported by mass spectrometry. ESI mass spectral peak of PYPH, $[PYPH + H^{+}]$ and PYPH:Hg^{2+} were at m/z = 350.15 $[C_{23}H_{18}N_4]$, 351.26 $[C_{23}H_{18}N_4{+}H]^{+}$ (Figure S2, supplementary material) and 937.87 $[C_{46}H_{34}HgN_4{+}K]^{+}$, respectively (Figure S7, supplementary material).

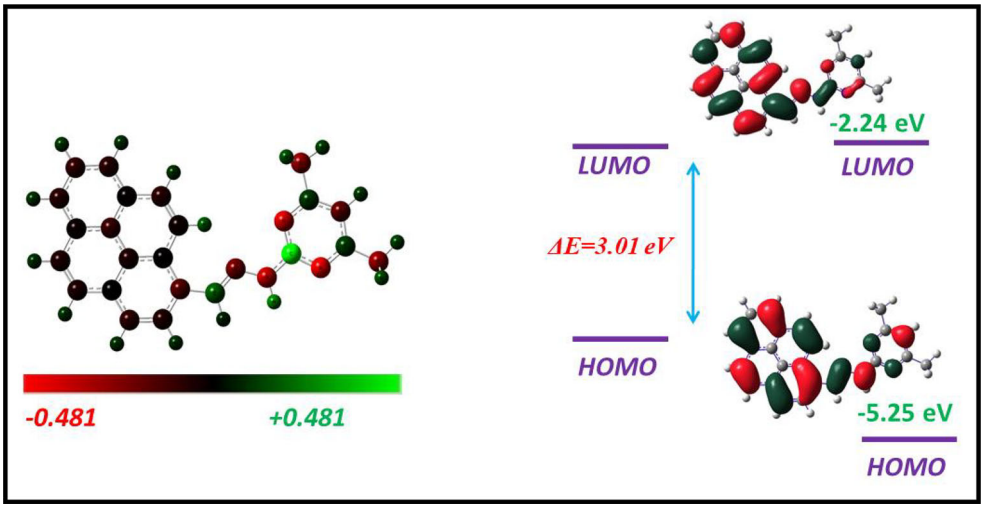

Figure 7. Ground state optimized structure of PYPH.

Table 2. Theoretical spectral data with the corresponding experimental absorption, dipole moment, energy of HOMO and LUMO of PYPH.

Theoretical λ_{abs}^{theo} (nm)	411.98
Oscillator strength (f)	0.7110
Experimental λ_{abs}^{exp} (nm)	398
Dipole Moment(μ) debye	1.5721
Energy of HOMO (eV)	−5.25
Energy of LUMO (eV)	−2.24
Energy gap (eV)	3.01

3.6. Theoretical calculations

Calculations of PYPH have been completed to understand the above experimental spectral properties. In the first step, ground state geometry of PYPH was optimized. Next, TD-DFT method has been applied to determine the transition energy and oscillator strength (f). The optimized geometrical structures with the Mulliken charge distribution (-0.481 to +0.481) and the HOMO-LUMO energy gap of 3.01 eV of PYPH is shown in Figure 7. The theoretical absorbance maximum of PYPH is 411.98 nm with oscillator strength (f) 0.7110 (Figure S8, supplementary material), which is close to the experimental findings (398 nm). Due to having different electronegative elements of PYPH molecule, a dipole moment (μ) of 1.5721 D is present (Table 2). The bond lengths of (26 C-28N), (28 N-29N), (29 N-31C), (32 N-31C), (31 C-35N), (32 N-34C) and (35 N-33C) of PYPH are 1.284 Å, 1.343 Å, 1.397 Å, 1.333 Å, 1.342 Å, 1.337 Å and 1.334 Å, respectively (Table 3). The bond angles of (<16 C-25C-28N), (<28 N-29N-31C) and the (<26 C-28N-29N) of PYPH are 125.7°, 123.2°, 117.5°, respectively (Table 3).

4. Conclusion

A Schiff base fluorescent chemosensor, PYPH, containing biologically active pyrimidine was synthesized and its sensing properties were investigated in aqueous solutions.

Table 3. Bond lengths and angles of PYPH.

Bond lengths (Å)	
(26C-28N)	1.284
(28N-29N)	1.343
(29N-31C)	1.397
(32N-31C)	1.333
(31C-35N)	1.342
(32N-34C)	1.337
(35N-33C)	1.334
Bond angles (°)	
(<16C-25C-28N)	125.7
(<28N-29N-31C)	123.2
(<26C-28N-29N)	117.5

The solvatochromic behavior of PYPH depends not only on polarity of the medium but also hydrogen bonding properties of the solvent. PYPH can be used as a fluorescent chemosensor for Hg^{2+} detection. The sensing mechanism based on nonfluorescent complexation between sensor PYPH and Hg^{2+} was confirmed by Job's plots and ESI mass spectra. Therefore, PYPH can serve as a potential sensor for quantitative detection of Hg^{2+} in different samples.

Acknowledgements

All the authors are thankful to Jadavpur University, Kolkata, India for the research facilities.

Disclosure statement

No potential conflict of interest was reported by the author(s).

Funding

S.C.B. acknowledges financial assistance from DST-SERB (grant no. EMR/2015/000678).

References

[1] M.Q. Zhu, L.Q. Wang, G.J. Exarhos, A.D.Q. Li. *J. Am. Chem. Soc.*, **126**, 2656 (2004).
[2] Toxic Substances Portal, *Agency for Toxic Substances and Disease Registry*, **60**, 1154 (2011).
[3] L. Feng, Y. Deng, X. Wang, M. Liu. *Sens. Actuators B*, **245**, 441 (2017).
[4] F. Yan, M. Wang, D. Cao, N. Yang, Y. Fu, L. Chen, L. Chen. *Dyes Pigm*, **98**, 42 (2013).
[5] X.F. Wu, Q.J. Ma, X.J. Wei, Y.M. Hou, X. Zhu. *Sens. Actuators B*, **183**, 565 (2013).
[6] Q. Yue, T. Shen, J. Wang, L. Wang, S. Xu, H. Li, J. Liu. *Chem. Commun. (Camb))*, **49**, 1750 (2013).
[7] H.N. Kim, W.X. Ren, J.S. Kim, J.S. Yoon. *Chem. Soc. Rev.*, **41**, 3210 (2012).
[8] E.M. Nolan, S.J. Lippard. *Chem. Rev.*, **108**, 3443 (2008).
[9] M. Saleem, M. Rafiq, M. Hanif. *J. Fluoresc.*, **27**, 31 (2017).
[10] J. Hu, Z. Hu, S. Liu, Q. Zhang, H.-W. Gao, K. Uvdal. *Sens. Actuators B*, **230**, 639 (2016).
[11] R.M. Shafeeulla, G. Krishnamurthy, H.S. Bhojynaik, H.P. Shivarudrappa, Y. Shiralgi. *Beni-Seuf Univ. J. Basic Appl. Sci*, **6**, 332 (2017).
[12] A. Naganuma, T. Furuchi, N. Miura, G.W. Hwang, S. Kuge. *Tohoku J. Exp. Med*, **196**, 65 (2002).

[13] B.O. Lund, D.M. Miller, J.S. Woods. *Biochem. Pharmacol.*, **45**, 2017(1993).
[14] M.A. Peraza, F. Ayala Fierro, D.S. Barber, E. Casarez, L.T. Rael. *Environ. Health Perspect*, **106**, 203 (1998).
[15] B.A. Babgi, A. Alzahrani. *J. Fluoresc.*, **26**, 1415 (2016).
[16] Z. Shokohi-Pour, H. Chiniforoshan, A.A. Momtazi-Borojeni, B. Notash. *J. Photochem. Photobiol. B.*, **162**, 34 (2016).
[17] J. Jiao, M. Jiang, Y.T. Li, Z.Y. Wu, C.W. Yan. *J. Biochem. Mol. Toxicol.*, **28**, 47 (2014).
[18] K.S. Kumar, C. Priya Varma. *J. Pharm. Sci. Res.*, **9**, 1317 (2017).
[19] A.S. El-Tabl, M.S. Ahmed Shahin. *IJAC*, **4**, 01 (2018).
[20] V. Gomathi, R. Selvameena. *Int. J. Recent Sci. Res.*, **4**, 94 (2013).
[21] K. Shivakumar, P. Shashidhar, P. Vithal Reddy, M.B. Halli. *J. Coord. Chem.*, **61**, 2274 (2008).
[22] N. Dharmaraj, P. Viswanathamurthi, K. Natarajan. *Transition Met. Chem.*, **26**, 105 (2001).
[23] E.G. Stoddard, B.J. Killinger, S.A. Nag, J. Martin, R. Corley, J.N. Smith, A.T. Wright. *Chem. Res. Toxicol.*, **32**, 1259 (2019).
[24] J.A. Cullen, C.D. Marshall, D. Hala. *Sci. Total Environ.*, 650, 1158 (2019).
[25] R. Kumar, R. Ramesh, J.G. Małecki. *J. Organomet. Chem.*, 862, 95 (2018).
[26] A.I. Vogel. *Textbook of Practical Organic Chemistry*, 5th Edn, p. 397. Singapore Publishers Ltd., Singapore, London (1994).
[27] S. Gupta, S. Roy, T.N. Mandal, K. Das, S. Ray, R.J. Butcher, S.K. Kar. *J. Chem. Sci.*, **122**, 1 (2010).
[28] S. Ghosh, D. Singharoy, A. Dhara, J.P. Naskar, S.C. Bhattacharya. *Eur. J. Inorg. Chem.*, **2018**, 2695 (2018).
[29] S. Ghosh, D. Singharoy, S.C. Bhattacharya. *Spectrochim. Acta, Part A: Mol. Biomol. Spectrosc.*, **195**, 7 (2018).
[30] P. Hohenberg, W. Kohn. *Phys. Rev.*, 136, B864(1964).
[31] W. Kohn, L.J. Sham. *Phys. Rev.*, 140, A1133(1965).
[32] A.D. Becke. *J. Chem. Phys.*, 98, 5648 (1993).
[33] C. Neiss, P. Saalfrank, M. Parac, S. Grimme. *J. Phys. Chem. A.*, 107, 140 (2003).
[34] D. Singharoy, S. Chowdhury, S.S. Mati, S. Ghosh, K. Chattopadhyay, S.C. Bhattacharya. *Chemistry*, 23, 16516 (2017).
[35] S. Dhar, D.K. Rana, S. Roy, S. Roy, S. Bhattacharya, S.C. Bhattacharya. *J. Luminesc.*, **132**, 957 (2012).
[36] Fluka. *Selectophore Catalog*, Kluwer Academic Publishers, Neu-Ulm (1996).
[37] R.P.; Haugland. *Handbook of Fluorescent Probes and Research Products, Molecular Probes*, Eugene (2001).
[38] A.W. Czarnik (Ed.), Fluorescent chemosensors for ion and molecule recognition, *ACS Symposium Series* 538. ACS Publication, Washington, DC (1992).
[39] W.T. Mason. Fluorescent and luminescent probes for biological activity. In *Biological Techniques*, D.B. Sattelle (Ed.), Academic Press, San Diego, CA (1999).
[40] Z. Xu, J. Yoon, D.R. Spring. *Chem. Soc. Rev.*, 39, 1996 (2010).
[41] S. Pal, B. Sen, M. Mukherjee, K. Dhara, E. Zangrando, S.K. Mandal, A.R. Khuda-Bukhsh, P. Chattopadhyay. *Analyst*, **139**, 1628 (2014).
[42] K. Aich, S. Goswami, S. Das, C.D. Mukhopadhyay. *RSC Adv.*, **5**, 31189(2015).
[43] J.R. Lakowicz. *In Principles of Fluorescence Spectroscopy*, Plenum Press, New York (1999).